Journal of Computational Physics 400 (2020) 108956

Contents lists available at ScienceDirect

Journal of Computational Physics

www.elsevier.com/locate/jcp

A level-set immersed interface method for simulating the electrohydrodynamics

Jian-Jun Xu [a], Weidong Shi [b,*], Wei-Fan Hu [c], Jun-Jie Huang [d]

[a] Chongqing Institute of Green and Intelligent Technology, Chinese Academy of Sciences, Chongqing, China
[b] School of Applied Mathematics, Shanxi University of Finance and Economics, Taiyuan, China
[c] Department of Applied Mathematics, National Chung Hsing University, Taichung, Taiwan
[d] School of Aerospace Engineering, Chongqing University, Chongqing, China

ARTICLE INFO

Article history:
Received 8 April 2019
Accepted 16 September 2019
Available online 27 September 2019

Keywords:
Level-set method
Immersed interface method
Electrohydrodynamics
Leaky dielectric model
Drop breakup
Drop coalescence

ABSTRACT

A method is proposed for simulating the electrohydrodynamics (EHD). The level-set method is used to capture the interface to take its advantage in handling topological change. In order to accurately solve the Poisson equation with interface jump conditions for the electric potential, a simple version of the level-set based immersed interface method (IIM) is developed. This version avoids the local coordinate transform in the original IIM in literature, reducing the complexity of the algorithm significantly. The IIM achieves second-order accuracy for both the electric potential and its gradient. A level-set extrapolation procedure is presented to calculate the electric surface force. Numerical simulations on drop deformation, breakup and coalescence in both 2D and 3D are presented.

1. Introduction

Applying an external electric field to manipulate suspended drops and bubbles has been an important means in numerous industrial processes, for example, ink-jet printing [5,34], oil extraction from oil-water emulsions [16], electrospraying [13], microfluidic devices [45] etc. Electrohydrodynamics (EHD) studies the fluid dynamics subjected to electric fields. It has gained a lot of research attention. Several numerical methods have been proposed for simulating the electrohydrodynamics, based on interface tracking methods, including the front-tracking method [6,22,20,14,35], the volume-of-fluid method [31], the level-set method [10,50,51], and hybrid volume-of-fluid-level-set method [52,21], etc.

In the numerical simulation of EHD, a key issue is to solve the Poisson equation for the electric potential with interface jump conditions (see eq. (13)). In the literature, several methods were used/developed to solve the potential Poisson equation, including the boundary integral method (BIM) [6,22,14], the weighted harmonic averaging method (WHAM) [52,51,31,21], the immersed interface method (IIM) [20,35], and the ghost fluid method (GFM) [10,50]. The BIM is accurate, however, it is based on the front tracking method. The front-tracking method explicitly tracks the interface using Lagrangian markers, and it may be difficult to deal with interfacial topological changes and 3D simulations. The WHAM is simple, however, it is only first-order accurate. Since the electric potential needs to be differentiated in calculating the surface electric force, the first-order accuracy may not be enough as pointed out in [20]. It was reported that the WHAM had zeroth-order accuracy for the gradient of the electric potential. To improve the accuracy, the authors in [20] developed a simplified version of the second-order accurate IIM. This version of IIM avoids the local coordinate transform in the original IIM [26,27,30,15] in

* Corresponding author.
E-mail addresses: xujianjun@cigit.ac.cn (J.-J. Xu), shiwd@sxufe.edu.cn (W. Shi), wfhu@dragon.nchu.edu.tw (W.-F. Hu), jjhuang@cqu.edu.cn (J.-J. Huang).

https://doi.org/10.1016/j.jcp.2019.108956
0021-9991/

constructing the finite difference scheme at the irregular grid points (i.e. grid points just adjacent to the interface), reducing the complexity of IIM significantly. In [20], however, the interface is explicitly tracked using the Lagrangian markers. It was shown in [20] that the IIM also achieved second-order accuracy for the potential gradient. This IIM was used in [35] for simulating EHD under the assumption of axisymmetric geometry. The GFM also pays special attention at the irregular grid points, however, it ignores the jump of the tangential flux [19]. Note that a finite volume method was proposed in [18] for solving more general elliptic equations with interface jump conditions. It was shown there that the finite volume method achieves second-order accuracy for the solution and first-order accuracy for the solution gradient.

There are several methods for solving the Navier-Stokes (N-S)/Stokes equations with singular surface forces in EHD simulations. The BIM was used in [6,22,14] for the Stokes equations. The BIM is not suitable for the nonlinear N-S equations, and it is based on the front-tracking method. Regardless of EHD simulation, level-set based IIM were used in [54,56] for solving the Stokes equations for the surfactant problem under the assumption that the viscosities of two phases are matched. The continuum surface force method (CSFM) [52,51,31,21], the GFM [10,50], and the IIM [35] were used for the N-S equations. The CSFM utilizes a discrete Dirac δ function to recast the N-S equations for two-phase flows as "one-fluid" formulation. Then the projection methods [9,12] can be used to solve the resultant N-S equations. The CSFM has been popular in computing two-phase flow problems due to its simplicity, e.g., [39,11,47,40,52,51,55,20,57], just list a few. The conventional wisdom is that the CSFM is first-order convergent. Note that second-order convergent methods for solving N-S equations with singular forces were proposed in literature regardless of EHD simulation. In [29,48] the IIM was used for solving the Poisson equations resulting from the projection method. In [8,25,35], the velocity is decomposed into a non-smooth "Stokes" part and a smooth regular part, and the IIM is used for the "Stokes" part to achieve second-order accuracy. These IIM-type N-S solvers need to derive jump conditions for the velocity and pressure, which can be complicated when the viscosities/densities of two-phases are unmatched. They were presented in 2D or axisymmetric 3D.

The level-set method [37,36] has become an invaluable tool for computing interface problems. The advantages of the level-set method include relatively easy implementation in 3D and the capability of handling interfacial topological changes. The purpose of this work is to present an efficient level-set method for simulating EHD in both 2D and 3D. In particular we develop a new level-set based IIM for solving the potential Poisson interface problem. Correspondingly level-set based techniques are proposed for calculating the surface electric force. The CSFM are used for solving the N-S equations with singular forces.

The paper is organized as follows. The mathematical formulation of the problem is stated in Section 2. The numerical methods are described in Section 3. Numerical tests of the methods and simulations on droplet dynamics under electric fields in both 2D and 3D are given in Section 4. Some concluding remarks are given in Section 5.

2. Mathematical formulation

2.1. Governing equations

We consider that an external electric field is applied to a system of two immiscible fluids, as illustrated in Fig. 1. The Navier-Stokes equations governing the fluid motion including the electric force read following:

$$\rho\left(\frac{\partial \mathbf{u}}{\partial t}+(\mathbf{u}\cdot\nabla)\mathbf{u}\right)=\nabla\cdot\mathbf{T}+\nabla\cdot\mathbf{M},\quad \text{in}\quad \Omega^{\pm}, \tag{1}$$

$$\nabla\cdot\mathbf{u}=0,\quad \text{in}\quad \Omega^{\pm}, \tag{2}$$

where $\mathbf{u}$ is the velocity field, p the pressure, $\mathbf{T}=-pI+\mu(\nabla\mathbf{u}+\nabla\mathbf{u}^T)$ the traditional deformation tensor, $\mathbf{M}$ the Maxwell electric stress tensor (described below). The far field velocity condition is $\mathbf{u}|_{\partial\Omega}=\mathbf{u}_\infty$.

The leaky dielectric model [32,42] is used for the electric equations. The dynamic currents are small so the related magnetic effect can be ignored. Thus the electric field density $\mathbf{E}$ is irrotational, i.e., $\nabla\times\mathbf{E}=0$ in $\Omega^{\pm}$. $\mathbf{E}$ can be rewritten as $\mathbf{E}=-\nabla\psi$, here ψ is the electric potential. The volume charge density q_v can be expressed as $q_v=\nabla\cdot(\epsilon\mathbf{E})$ with the permittivity ϵ. The charge conservation equation is

$$\frac{Dq_v}{Dt}+\nabla\cdot(\sigma\mathbf{E})=0,\quad \text{in}\quad \Omega^{\pm}, \tag{3}$$

where σ is the electric conductivity, $\frac{D}{Dt}=\frac{\partial}{\partial t}+\mathbf{u}\cdot\nabla$ is the material derivative.

It is known that the relaxation time scale for the charge decay is $t^e=\epsilon/\sigma$ (see, e.g., [32,42,52]). The viscous time scale of the fluid motion is $t^v=\rho R^2/\mu$, where R is the characteristic length scale. We assume that the two fluids are leaky dielectric so that the volume charges reach steady state in a much shorter time than the fluid, i.e., $t^e\ll t^v$. The volume charges accumulate on the interface almost instantly. Then eq. (3) is simplified to a Poisson equation for the potential ψ:

$$\nabla\cdot(\sigma\nabla\psi)=0,\quad \text{in}\quad \Omega^{\pm}, \tag{4}$$

with the boundary conditions

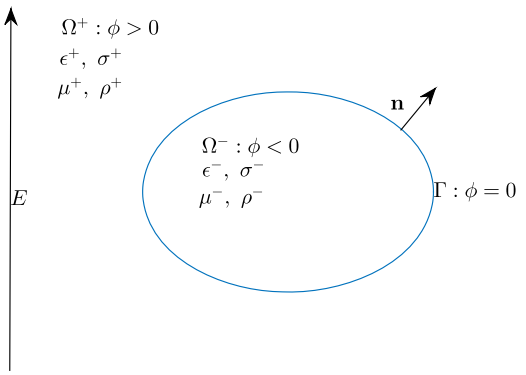

Fig. 1. A configuration of the electric two-phase flow: ϕ is the level-set function representing the interface Γ. The normal of the interface $\mathbf{n} = \frac{\nabla\phi}{|\nabla\phi|}$ points into the bulk fluid. Piecewise constant quantities $\sigma, \epsilon, \mu, \rho$ represent respectively the electric conductivity, the permittivity, the fluid viscosity, and the density.

$$[\psi] = 0, \quad \left[\sigma \frac{\partial \psi}{\partial \mathbf{n}}\right] = 0, \tag{5}$$

where notation $[\cdot]$ represents a jump across the interface, which is defined as the limit from Ω^+ side minus the limit from Ω^- side.

The electric force acts only on the interface Γ. A force balance on the interface among the viscous force, the electric force and the surface tension force leads to the following interface jump condition:

$$[\mathbf{Tn}] + [\mathbf{Mn}] = \gamma\kappa\mathbf{n}, \tag{6}$$

where γ is the surface tension, $\kappa = \nabla \cdot \mathbf{n}$ the mean curvature, $\mathbf{M} = \epsilon\left(\mathbf{EE} - \frac{1}{2}(\mathbf{E}\cdot\mathbf{E})I\right)$ the Maxwell stress tensor.

The jump condition (6) can be regarded as singular surface forces and naturally included into the momentum equation via the level-set function ϕ and the Dirac δ function. Consequently, we have a unified momentum equation on the whole domain $\Omega = \Omega^+ \cup \Omega^- \cup \Gamma$ as follows.

$$\rho\left(\frac{\partial \mathbf{u}}{\partial t} + (\mathbf{u}\cdot\nabla)\mathbf{u}\right) = \nabla\cdot\mathbf{T} + (-\gamma\kappa\mathbf{n} + [\mathbf{Mn}])\delta(\phi)|\nabla\phi|, \quad \text{in} \quad \Omega. \tag{7}$$

The velocity $\mathbf{u}$ is continuous across the interface. The interface moves with the fluid velocity leading to the level-set convection equation:

$$\frac{\partial \phi}{\partial t} + \mathbf{u}\cdot\nabla\phi = 0. \tag{8}$$

In practice the level-set function is re-initialized to be a signed distance function by solving the following Hamilton-Jacobi equation [47] as

$$\begin{cases} \dfrac{\partial \phi}{\partial \tau} + S(\phi_0)(|\nabla\phi| - 1) = 0, \\ \phi(\mathbf{x}, 0) = \phi_0(\mathbf{x}), \end{cases} \tag{9}$$

where τ is a pseudo-time, ϕ_0 is the level-set function obtained from solving Eq. (8), and $S(\cdot)$ is the sign function as follows:

$$S(x) = \begin{cases} 1, & \text{if} \quad x > 0, \\ 0, & \text{if} \quad x = 0, \\ -1, & \text{if} \quad x < 0. \end{cases} \tag{10}$$

2.2. Dimensionless equations

The physical variables are scaled by the corresponding characteristic quantities. We still use the same notations for the same variables after the non-dimensionalization. Specifically we define

$$\mathbf{x} := \frac{\mathbf{x}}{R}, \quad t := \sqrt{\frac{\gamma_0}{\rho^+ R^3}}t, \quad p := \frac{pR}{\gamma_0}, \quad \rho := \frac{\rho}{\rho^+}, \quad \mu = \frac{\mu}{\mu^+},$$
$$\gamma := \frac{\gamma}{\gamma_0}, \quad \epsilon := \frac{\epsilon}{\epsilon^+}, \quad \sigma := \frac{\sigma}{\sigma^+}, \quad \mathbf{E} := \frac{\mathbf{E}}{E_0}.$$

Here R and γ_0 are initial radius and the characteristic surface tension of the droplet, respectively. E_0 is the characteristic magnitude of the electric field intensity.

For simplicity, we assume in this work that the viscosities and densities of two fluids are matched so that $\rho = \mu = 1$ after the non-dimensionalization.

The Navier-Stokes equations becomes

$$\frac{\partial \mathbf{u}}{\partial t} + (\mathbf{u}\cdot\nabla)\mathbf{u} = -\nabla p + Oh\Delta\mathbf{u} + \mathbf{F}, \quad \text{in} \quad \Omega, \tag{11}$$

where $\mathbf{F} = (-\gamma\kappa\mathbf{n} + Ca_E[\mathbf{Mn}])\delta(\phi)|\nabla\phi|$ represents the singular surface force: the first term corresponds to the surface tension force and the second term the surface electric force. $\mathbf{M} = \epsilon\left(\mathbf{EE} - \frac{1}{2}(\mathbf{E}\cdot\mathbf{E})I\right)$. Here $\epsilon = \epsilon^-/\epsilon^+$ is the ratio of permittivity. The Ohnesorge number $Oh = \mu^+/\sqrt{\gamma_0\rho^+R}$ indicates the ratio of viscous force to surface tension force. The electric capillary number $Ca_E = R\epsilon^+E_0^2/\gamma_0$ reflects the strength of the external electric field.

The dimensionless continuity equation is

$$\nabla\cdot\mathbf{u} = 0, \quad \text{in} \quad \Omega. \tag{12}$$

The Poisson equation for the dimensionless electric potential ψ is

$$\Delta\psi = 0, \quad \text{in} \quad \Omega^{\pm}, \tag{13}$$

together with the interface jump conditions

$$[\psi] = 0, \quad \left[\sigma\frac{\partial\psi}{\partial\mathbf{n}}\right] = 0, \tag{14}$$

where $\sigma = \sigma^-/\sigma^+$ is the ratio of conductivity.

3. Numerical methods

In this section, we describe the numerical methods for solving the involved equations. We describe the method in 2D. Roughly speaking, the extension to 3D is simply adding one more dimension due to the level-set representation of the interface. Lay down a uniform mesh with grid length h on the computational domain $\Omega = [a,b]\times[c,d]$, with grid points $\mathbf{x}_{ij} = (a+ih, b+jh)^T, i = 0,1,\cdots,M, j = 0,1,\cdots,N$. Time marches uniformly with time step Δt, with time instants $t^n = n\Delta t$.

3.1. Continuum surface force method for the Navier-Stokes equations

We assume that the viscosity ratio and density ratio are 1. One can use the method in [55] for general two-phase flows. The δ function is regularized as

$$\delta(x) \approx \delta_{\epsilon_0}(x) = \begin{cases} \frac{1}{2\epsilon_0}(1+\cos(\frac{\pi x}{\epsilon_0})), & \text{if} \quad |x| \le \epsilon_0, \\ 0, & \text{otherwise}, \end{cases} \tag{15}$$

with $\epsilon_0 = 1.5h$.

The projection method (e.g., [12]) is used for Navier-Stokes equations (11) and (12). It consists of the following three steps in marching from time t^n to t^{n+1}.

First an intermediate velocity $\mathbf{u}^*$ is solved as

$$\frac{\mathbf{u}^* - \mathbf{u}^n}{\Delta t} + \frac{3}{2}((\mathbf{u}\cdot\nabla)\mathbf{u})^n - \frac{1}{2}((\mathbf{u}\cdot\nabla)\mathbf{u})^{n-1} + \nabla p^{n-\frac{1}{2}} = \frac{Oh}{2}(\Delta\mathbf{u}^* + \Delta\mathbf{u}^n) + \mathbf{F}^{n+\frac{1}{2}}, \tag{16}$$

with Dirichlet boundary condition $\mathbf{u}^*|_{\partial\Omega} = \mathbf{u}_\infty$. Next we project the intermediate velocity $\mathbf{u}^*$ into the divergence free space by first solving the following Poisson equation for an auxiliary function χ:

$$\Delta\chi = \frac{\nabla\cdot\mathbf{u}^*}{\Delta t}, \qquad \frac{\partial\chi}{\partial\mathbf{n}}\Big|_{\partial\Omega} = 0, \tag{17}$$

and then updating the velocity by

$$\mathbf{u}^{n+1} = \mathbf{u}^* - \Delta t\nabla\chi. \tag{18}$$

Lastly, the pressure gradient is updated by

$$\nabla p^{n+\frac{1}{2}} = \nabla p^{n-\frac{1}{2}} + \nabla\chi. \tag{19}$$

In the above, standard centered difference schemes are used for the spatial derivatives discretization, except that the third-order WENO scheme [44] is used for the nonlinear convection terms $((\mathbf{u}\cdot\nabla)\mathbf{u})^n$ and $((\mathbf{u}\cdot\nabla)\mathbf{u})^{n-1}$.

3.2. Level-set based immersed interface method for the elliptic interface equation

The electric Potential equation (13) with jump condition (14) is solved by using a level-set based immersed interface method. Here we consider more general elliptic interface problem:

$$\nabla \cdot (\beta \nabla u) = \tilde{f}, \quad \text{in} \quad \Omega - \Gamma, \tag{20}$$

with jump conditions

$$[u] = v, \quad [\beta u_n] = w, \quad \text{on} \quad \Gamma. \tag{21}$$

Assume that the diffusion coefficient β is piecewise constant in Ω. Without the loss of generality we assume that $\beta \equiv \beta^+$ in Ω^+, and $\beta \equiv 1$, in Ω^-. Note that $[\beta] = \beta^+ - 1$. In reality the jump conditions are physically meaningful only at the interface Γ. However, in the level-set technology the interface quantities are often implicitly defined at the grid points in a small neighborhood of the interface. Therefore we assume that the jumps v, w are given as smooth functions defined in a small neighborhood of the interface Γ, similar as in [56].

The elliptic equation (20) can be rewritten as

$$\Delta u = f \equiv \begin{cases} \dfrac{\tilde{f}^+}{\beta^+}, & \text{in} \quad \Omega^+, \\ \tilde{f}^-, & \text{in} \quad \Omega^-. \end{cases} \tag{22}$$

Similar as in [30,58,20], we make the following choices which make the resulting linear system (i.e. eq. (38)) more diagonally dominant. If $[\beta] < 0$, then we rewrite the flux jump condition $[\beta u_n] = w$ as

$$u_n^+ + \frac{1}{[\beta]}[u_n] = \frac{w}{[\beta]}. \tag{23}$$

Otherwise, we rewrite is as

$$u_n^- + \frac{\beta^+}{[\beta]}[u_n] = \frac{w}{[\beta]}. \tag{24}$$

Though (23) and (24) are equivalent mathematically, numerical evidences indicate that the above choices can lead to significantly faster convergence of the iterative method for solving the discretized linear system.

3.2.1. Modified centered difference scheme

We first divide the grid points into two groups. If

$$\max\{\phi_{ij}, \phi_{i+1,j}, \phi_{i-1,j}, \phi_{i,j+1}, \phi_{i,j-1}\} > 0, \text{ and } \min\{\phi_{ij}, \phi_{i+1,j}, \phi_{i-1,j}, \phi_{i,j+1}, \phi_{i,j-1}\} \le 0,$$

then $\mathbf{x}_{ij}$ is irregular. Otherwise, it is regular.

If $\mathbf{x}_{ij}$ is regular, then standard centered difference scheme is used to discretize (22):

$$\frac{u_{i+1,j} + u_{i-1,j} + u_{i,j+1} + u_{i,j-1} - 4u_{ij}}{h^2} = f_{ij} + O(h^2). \tag{25}$$

Next let $\mathbf{x}_{ij}$ be an irregular grid point. We need to modify the centered difference scheme due to the jump discontinuity of u across the interface. If the local truncation error of the modified centered difference scheme at all the irregular grid points is $O(h)$, the whole finite difference method is still uniformly accurate to $O(h^2)$ [7].

In the construction of the modified finite difference scheme at irregular grid points, we borrow the idea from [20,24]. The implementation details are different, since we use the level-set representation of the interface.

Let $\mathbf{x}_{lk} \neq \mathbf{x}_{ij}$ be any grid point involved in the centered difference scheme at $\mathbf{x}_{ij}$, and $\mathbf{x}_{lk}$ and $\mathbf{x}_{ij}$ are on different side of the interface, more precisely, $\tilde{S}(\phi_{lk})\tilde{S}(\phi_{ij}) < 0$. Here $\tilde{S}$ is the modified sign function given by

$$\tilde{S}(x) = \begin{cases} 1, & \text{if} \quad x > 0, \\ -1, & \text{if} \quad x \le 0. \end{cases} \tag{26}$$

For easy presentation, we denote $\mathbf{x} \equiv \mathbf{x}_{lk}, u \equiv u(\mathbf{x}_{lk})$. Assume that the solution is smoothly extended from $\mathbf{x}_{ij}$ side of the interface to the other side. Denote the extended solution at $\mathbf{x}$ as $\tilde{u}$. Then we have

$$u - u_{ij} = (\tilde{u} - u_{ij}) + (u - \tilde{u}). \tag{27}$$

The first term on the right hand side of (27) fits the standard centered scheme (25) for the extended smooth function. We need to find an approximation of the second term to $O(h^3)$. The approximation will determine the correction term in the modified difference scheme.

First we find the projection point $\mathbf{x}^*$ of $\mathbf{x}$ on interface along the normal direction, i.e., $\mathbf{x}^* = \mathbf{x} + \alpha\mathbf{n}$. Here α is determined by solving the following quadratic equation as in [30,56]:

$$\phi(\mathbf{x}) + \alpha|\nabla\phi(\mathbf{x})| + \frac{\alpha^2}{2}\mathbf{n}(\mathbf{x})^T He(\phi(\mathbf{x}))\mathbf{n}(\mathbf{x}) = 0, \tag{28}$$

where He is the Hessian matrix.

Applying Taylor expansion to u and $\tilde{u}$ at $\mathbf{x}^*$, we have

$$u - \tilde{u} = -\tilde{S}(\phi_{ij})([u] - \alpha[u_n] + \frac{\alpha^2}{2}[u_{nn}]) + O(h^3). \tag{29}$$

In the above, the jumps $[u], [u_n], [u_{nn}]$ are evaluated at the projection point $\mathbf{x}^*$. Unknown $[u_n]$ is taken as an augmented variable, which will be solved together with the u. Unknown $[u_{nn}]$ can be expressed as follows.

Recall the surface gradient operator $\nabla_s = (I - \mathbf{n}\mathbf{n}^T)\nabla$ and the decomposition formula $\nabla_s^2 u = \Delta u - \frac{\partial^2 u}{\partial \mathbf{n}^2} - \kappa\frac{\partial u}{\partial \mathbf{n}}$ [53]. We have from (22)

$$\Delta u = \nabla_s^2 u + \kappa u_n + u_{nn} = f. \tag{30}$$

Thus

$$[u_{nn}] = [f] - \nabla_s^2[u] - \kappa[u_n]. \tag{31}$$

Consequently, the modified centered difference scheme at irregular $\mathbf{x}_{ij}$ is following:

$$\frac{u_{i+1,j} + u_{i-1,j} + u_{i,j+1} + u_{i,j-1} - 4u_{ij}}{h^2} = f_{ij} + C_{ij} + O(h), \tag{32}$$

where the correction term $C_{ij} = \sum_{lk} c_{lk}$, and

$$c_{lk} = \frac{1}{h^2}\tilde{S}(\phi_{ij})\left([u] + \frac{\alpha^2}{2}\left([f] - \nabla_s^2[u]\right) - \alpha[u_n] - \frac{\alpha^2}{2}\kappa[u_n]\right). \tag{33}$$

Standard centered difference schemes are used for the discretization of the normal $\mathbf{n}$ and the curvature κ.

3.2.2. Onesided extrapolation for $u_n^{\pm}$ at the projection points

The jump relation (23) or (24) is used to get equations for the augmented variable $[u_n]$ at the projection points. u_n^+ or u_n^- at the projection points are expressed in terms of u by using onesided extrapolation, as described below.

Suppose that we want to express u_n^- at a projection point $\mathbf{x}^* = (x^*, y^*)$ in terms of u at the grid points. If $x_{i_0} \le x^* < x_{i_0+1}$, and $y_{j_0} \le y^* < y_{j_0+1}$, then the extrapolation stencil is chosen as in the following pseudo code:

```
Do  i = i0 − 4, i0 + 4
Do  j = j0 − 4, j0 + 4
    If φij ≤ 0, then xij is selected.
End Do
End Do
```

Denote the selected grid points as $\mathbf{x}_i (i = 1, ..., m_0)$. We construct a cubic polynomial $P_3(\mathbf{x}) = c_0 + c_1 x + c_2 y + c_3 x^2 + c_4 xy + c_5 y^2 + c_6 x^3 + c_7 x^2 y + c_8 xy^2 + c_9 y^3$, such that

$$P_3(\mathbf{x}_i) = u(\mathbf{x}_i),\ i = 1, ..., m_0. \tag{34}$$

Rewrite (34) in matrix form as

$$\bar{A}\bar{c} = \bar{b}, \tag{35}$$

where $\bar{c} = (c_0, ..., c_9)^T$. The least square solution of (35) satisfies

$$\bar{A}^T\bar{A}\bar{c} = \bar{A}^T\bar{b}, \tag{36}$$

which is solved by using a standard SVD decomposition of $\bar{A}$.

Once P_3 is determined, $u_n^-(\mathbf{x}^*) = (\nabla P_3 \cdot \mathbf{n})(\mathbf{x}^*)$, here $\mathbf{n}(\mathbf{x}^*)$ is calculated by standard cubic interpolation since $\mathbf{n}$ is smooth across the interface. The onesided extrapolation for u_n^+ is similar.

Remark. If there are not enough grid points in the stencil for the cubic extrapolation (for example, when two drops are in near contact), we simply use the linear extrapolation.

3.2.3. Solving the resultant linear system

The resultant linear system consists of the standard centered difference equations (25) at the regular grid points, the modified centered difference equations (32) at the irregular grid points, and equation (23) or (24) discretized by the onesided extrapolation for u_n^+ (or u_n^-) at the projection points.

Let U, Ψ be the solution vector formed by u_{ij} and the augmented variable $[u_n]$, respectively. Then we have the matrix form of the discrete linear system:

$$\begin{cases} AU + E\Psi = F, \\ BU + \lambda\Psi = G_0. \end{cases} \tag{37}$$

In the above, AU corresponds to the standard centered difference scheme, $-E\Psi$ represents the terms involving $[u_n]$ in the correction term C_{ij}, F consists of the right hand side of (22) and the other known terms in C_{ij}. If $[\beta] < 0$, then BU represents the one-sided extrapolation for u_n^+ at the projection point, $\lambda = 1/[\beta]$. Otherwise, BU represents the one-sided extrapolation for u_n^- at the projection point, $\lambda = \beta^+/[\beta]$. G_0 corresponds to the vector of $w/[\beta]$ at the projection points.

We might use the BICGSTAB method [41] to solve the non-symmetric linear system (37). However, the convergence would be slow due to the large size of the system. In order to utilize the fast Poisson solver such as FFT [1], the iterative method is only applied to a small linear system for Ψ. To proceed, we eliminate U in the system (37) and get

$$\left(BA^{-1}E - \lambda I\right)\Psi = B(A^{-1}F) - G_0. \tag{38}$$

The BICGSTAB method is applied to solve (38), in which FFT is used to calculate $A^{-1}F$ and $A^{-1}E\Psi$.

Once we get Ψ, FFT is used to solve equation $AU = F - E\Psi$ to get the solution U. Note that in practice, we do not need to form the matrices such as A, B, E explicitly, since only the matrix-vector product is needed in the BICGSTAB iteration.

3.3. Calculating the electric force [**Mn**]

Once the electric potential ψ is available, standard centered difference scheme is used to calculate the electric field density $\mathbf{E} = -\nabla\psi$ at the regular grid points. At the irregular grid points we need to add a correction term to the centered difference scheme due to the jump discontinuity of ψ. Let $\mathbf{x}_{ij}$ be an irregular grid point. As before we imagine that ψ is smoothly extended from the $\mathbf{x}_{ij}$ side of the interface to the other side, and denote the extended smooth solution as $\tilde{\psi}$. Then we write

$$\frac{\psi_{i+1,j} - \psi_{i-1,j}}{2h} = \frac{\psi_{i+1,j} - \tilde{\psi}_{i+1,j}}{2h} + \frac{\tilde{\psi}_{i+1,j} - \tilde{\psi}_{i-1,j}}{2h} - \frac{\psi_{i-1,j} - \tilde{\psi}_{i-1,j}}{2h}. \tag{39}$$

In the above, the second term on the right hand side is the standard centered difference approximation to $\frac{\partial\psi}{\partial x}(\mathbf{x}_{ij})$ with truncation error $O(h^2)$. Thus we have

$$\frac{\partial\psi}{\partial x}(\mathbf{x}_{ij}) = \frac{\psi_{i+1,j} - \psi_{i-1,j}}{2h} + \left(-\frac{\psi_{i+1,j} - \tilde{\psi}_{i+1,j}}{2h} + \frac{\psi_{i-1,j} - \tilde{\psi}_{i-1,j}}{2h}\right) + O(h^2). \tag{40}$$

The term in the above parenthesis is the correction term which can be calculated by using (29), leading to a truncation error of $O(h^2)$. The calculation of $\frac{\partial\psi}{\partial y}(\mathbf{x}_{ij})$ is similar.

The normal Maxwell tensor **Mn** is directly calculated at all grid points in a small neighborhood of the interface.

We calculate the jump [**Mn**] using the PDE based extrapolation (or extension) technique as follows. Denote $\mathbf{Mn} = (M_1, M_2)^T$. The following first-order PDE is solved to extrapolate **Mn** from Ω^- side to Ω^+ side:

$$\frac{\partial\tilde{M}_i}{\partial\tau} + S(\phi + h)\mathbf{n}\cdot\nabla\tilde{M}_i = 0, i = 1, 2 \tag{41}$$

where initially $\tilde{M}_i = M_i, i = 1, 2$.

Likewise, another PDE is solved to extrapolate **Mn** from Ω^+ side to Ω^- side:

$$\frac{\partial\bar{M}_i}{\partial\tau} - S(\phi - h)\mathbf{n}\cdot\nabla\bar{M}_i = 0, i = 1, 2 \tag{42}$$

where initially $\bar{M}_i = M_i, i = 1, 2$. Note that several efficient high-order PDE based level-set extrapolation methods were proposed in [3,4]. Since we do not differentiate the electric force, the first-order extrapolation is enough, as indicated in the numerical experiments.

Then $[\mathbf{Mn}] = (\bar{M}_1 - \tilde{M}_1, \bar{M}_2 - \tilde{M}_2)^T\mathbf{n}$. Here [**Mn**] is a grid function calculated in a small neighborhood of the interface, only the part in the support of the discrete δ function serves for the electric force.

3.4. The global algorithm for the EHD

Given $\phi, \mathbf{u}, p$ and far field boundary conditions for ψ and $\mathbf{u}$ at time t^n, the global algorithm for the evolution to time t^{n+1} consists of the following steps:

- Step 1. Solve Poisson equations (13) with jump condition (14) using the immersed interface method to get the electric potential ψ.
- Step 2. Calculate the electric field $\mathbf{E}$, the Maxwell tensor $\mathbf{M}$, and the electric force [$\mathbf{Mn}$]; Calculate the surface tension force $-\gamma\kappa\mathbf{n}$.
- Step 3. Solve the Navier-Stokes equations (11) and (12) to get the velocity field $\mathbf{u}$.
- Step 4. Solve the level-set convection equation (8) and the reinitialization equation (9) to update the level-set function ϕ.

In the Step 4, the level-set equations can be solved by using either the Eulerian method (e.g., [53,33,59]) or the semi-Lagrangian method (e.g., [46,23,43,59]). Here we implement the Eulerian method. Moreover, the local level-set technique [38,53] is used, i.e. the level-set equations are solved in small tubes around the interface.

4. Numerical results

We first present examples for checking the accuracy of the level-set based immersed interface method, estimating the convergence rate of the global method for the EHD. Then we perform simulations on drop deformation, breakup and coalescence in both 2D and 3D. In the simulations we assume that the far-field boundary conditions for the electric potential is Dirichlet on the top and bottom sides: $\psi = y$ (or $\psi = z$ in 3D), and homogeneous Neumann boundary condition on the other sides. The velocity field vanishes in the far-field (i.e. $\mathbf{u}_\infty = 0$). Consequently the flow motion is driven by the applied electric field.

4.1. Accuracy check for the immersed interface method

We consider the elliptic equation (22) with jump conditions (21). We fix $\beta^- = 1$ and vary β^+. The error for the solution is measured by $\|u - u_h\|_\infty$. And the error for the gradient of solution is measured by $\|u_x - (u_h)_x\|_\infty + \|u_y - (u_h)_y\|_\infty$, where the numerical gradient is calculated by using the modified centered difference scheme in Sect. 3.3. In BICGSTAB iterations, the termination criterion is that the L_2 norm of the residual vector is not bigger than h^2. The initial guess for $[u_n]$ is 0.

Example 1. The computational domain is $\Omega = (-2, 2)^2$. The interface Γ is represented by the level-set function $\phi = \sqrt{(x/1.5)^2 + y^2} - 1$. The exactly solution is

$$u = \begin{cases} u^+ = \cos x \cos y, & \text{in} \quad \Omega^+, \\ u^- = \sin x \sin y, & \text{in} \quad \Omega^-. \end{cases} \tag{43}$$

The jump functions v, w are given as:

$$v = \begin{cases} u^+ - u^-, & \text{if} \quad |\phi(x, y)| \le 6h \\ 0, & \text{otherwise}, \end{cases} \tag{44}$$

$$w = \begin{cases} (\beta^+ \nabla u^+ - \beta^- \nabla u^-) \cdot \frac{\nabla \phi}{|\nabla \phi|}, & \text{if} \quad |\phi(x, y)| \le 6h, \\ 0, & \text{otherwise}, \end{cases} \tag{45}$$

Neumann boundary conditions are imposed on two horizontal sides. Dirichlet boundary conditions are imposed on two vertical sides.

Results for different β^+ are given in Tables 1 and 2. Second-order accuracy is achieved for both the solution and gradient.

Example 2. Same setting as in Example 1 except that a flower interface is chosen, see Fig. 2. The level-set function is $\phi = r - 1.0 - (y^5 + 5x^4 y - 10x^2 y^3)/(5r^5), r = \sqrt{x^2 + y^2}$. The mesh refinement results for different values of β^+ are given in Tables 3 and 4. When $\beta = 0.001$, the order of accuracy is poor for coarse grid, but it is improved as mesh is refined. For the other cases, second-order accuracy for both the solution and gradient is observed.

Example 3. The computational domain is $\Omega = [-2, 2]^3$. An ellipsoidal interface is chosen for which the level-set function is $\phi = \sqrt{(x/0.8)^2 + y^2 + (z/0.5)^2} - 1$. The exactly solution is

$$u = \begin{cases} u^+ = \cos x \cos y \cos z, & \text{in} \quad \Omega^+, \\ u^- = \sin x \sin y \sin z, & \text{in} \quad \Omega^-. \end{cases} \tag{46}$$

The right hand side $\tilde{f}$ and the jump functions are given exactly. Dirichlet boundary conditions are imposed on $\partial\Omega$. Mesh refinement results for different values of β^+ are shown in Tables 5 and 6. Again second-order accuracy is achieved for both the solution and gradient.

Table 1
Errors for the solution and gradient together with the convergence rates.

h	$\beta^+ = 0.001$				$\beta^+ = 0.1$			
	Solution error	Rate	Gradient error	Rate	Solution error	Rate	Gradient error	Rate
1/32	2.35×10^{-2}		6.57×10^{-2}		6.91×10^{-4}		1.51×10^{-3}	
1/64	1.15×10^{-2}	1.03	3.30×10^{-2}	1.00	1.53×10^{-4}	2.17	3.85×10^{-4}	1.97
1/128	3.06×10^{-3}	1.91	8.79×10^{-3}	1.91	3.58×10^{-5}	2.10	8.91×10^{-5}	2.11
1/256	7.37×10^{-4}	2.06	2.12×10^{-3}	2.05	8.44×10^{-6}	2.08	2.09×10^{-5}	2.09
1/512	1.86×10^{-4}	1.99	5.33×10^{-4}	1.99	2.14×10^{-6}	1.98	5.52×10^{-6}	1.92

Table 2
Errors for the solution and gradient together with the convergence rates.

h	$\beta^+ = 10$				$\beta^+ = 1000$			
	Solution error	Rate	Gradient error	Rate	Solution error	Rate	Gradient error	Rate
1/32	1.32×10^{-4}		3.37×10^{-4}		1.33×10^{-4}		3.84×10^{-4}	
1/64	2.88×10^{-5}	2.19	9.33×10^{-5}	1.85	3.06×10^{-5}	2.13	1.00×10^{-4}	1.94
1/128	6.76×10^{-6}	2.09	2.09×10^{-5}	2.16	7.09×10^{-6}	2.11	2.24×10^{-5}	2.16
1/256	1.66×10^{-6}	2.02	4.87×10^{-6}	2.10	1.69×10^{-6}	2.07	5.17×10^{-6}	2.11
1/512	4.41×10^{-7}	1.91	1.34×10^{-6}	1.86	4.66×10^{-7}	1.85	1.45×10^{-6}	1.83

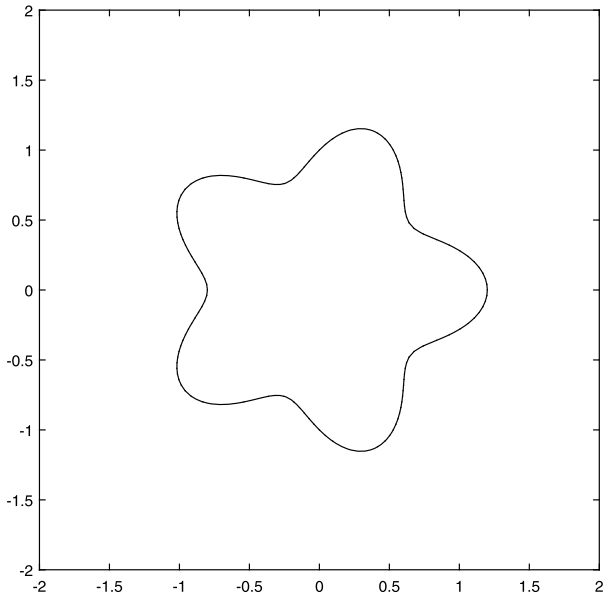

Fig. 2. The flower interface.

Table 3
Errors for the solution and gradient together with the convergence rates.

h	$\beta^+ = 0.001$				$\beta^+ = 0.1$			
	Solution error	Rate	Gradient error	Rate	Solution error	Rate	Gradient error	Rate
1/32	1.54×10^{-3}		3.48×10^{-3}		5.59×10^{-4}		2.03×10^{-3}	
1/64	1.99×10^{-3}	−0.37	5.60×10^{-3}	−0.69	9.40×10^{-5}	2.57	4.33×10^{-4}	2.23
1/128	1.32×10^{-3}	0.60	3.71×10^{-3}	0.60	2.72×10^{-5}	1.79	9.04×10^{-5}	2.26
1/256	5.43×10^{-4}	1.28	1.54×10^{-3}	1.27	7.07×10^{-6}	1.94	2.09×10^{-5}	2.11
1/512	1.53×10^{-4}	1.83	4.35×10^{-4}	1.82	1.85×10^{-6}	1.94	5.37×10^{-6}	1.96

4.2. A mesh refinement study for the global method

The computational domain is $\Omega = [-4, 4]^2$. Initially the drop is a unit circle centered at the origin. The physical parameters are chosen as $\sigma = 4, \epsilon = 3.5, Ca_E = 1, Oh = 1$. Since the exact solutions for the physical variables are unknown, we estimate the convergence rate r_q for a physical quantity q based on the computational results using three grid lengths according to the following formula:

Table 4
Errors for the solution and gradient together with the convergence rates.

h	$\beta^+ = 10$				$\beta^+ = 1000$			
	Solution error	Rate	Gradient error	Rate	Solution error	Rate	Gradient error	Rate
1/32	1.58×10^{-4}		2.00×10^{-3}		1.80×10^{-4}		2.13×10^{-3}	
1/64	3.25×10^{-5}	2.28	4.73×10^{-4}	2.08	3.60×10^{-5}	2.33	4.92×10^{-4}	2.11
1/128	6.79×10^{-6}	2.26	7.34×10^{-5}	2.69	7.48×10^{-6}	2.27	7.76×10^{-5}	2.67
1/256	1.89×10^{-6}	1.85	1.50×10^{-5}	2.30	2.04×10^{-6}	1.88	1.59×10^{-5}	2.29
1/512	4.26×10^{-7}	2.15	3.48×10^{-6}	2.10	4.71×10^{-7}	2.11	3.64×10^{-6}	2.12

Table 5
Errors for the solution and gradient together with the convergence rates.

h	$\beta^+ = 0.001$				$\beta^+ = 0.1$			
	Solution error	Rate	Gradient error	Rate	Solution error	Rate	Gradient error	Rate
1/8	9.20×10^{-3}		4.03×10^{-2}		7.71×10^{-3}		3.43×10^{-2}	
1/16	2.10×10^{-3}	2.13	9.67×10^{-3}	2.06	1.35×10^{-3}	2.51	6.63×10^{-3}	2.37
1/32	6.64×10^{-4}	1.66	2.75×10^{-3}	1.81	2.13×10^{-4}	2.67	9.60×10^{-4}	2.79
1/64	2.04×10^{-4}	1.70	8.90×10^{-4}	1.63	2.81×10^{-5}	2.92	1.78×10^{-4}	2.43

Table 6
Errors for the solution and gradient together with the convergence rates.

h	$\beta^+ = 10$				$\beta^+ = 1000$			
	Solution error	Rate	Gradient error	Rate	Solution error	Rate	Gradient error	Rate
1/8	2.85×10^{-3}		2.45×10^{-2}		3.28×10^{-3}		2.90×10^{-2}	
1/16	5.78×10^{-4}	2.30	4.63×10^{-3}	2.40	6.62×10^{-4}	2.31	5.42×10^{-3}	2.42
1/32	9.94×10^{-5}	2.54	6.81×10^{-4}	2.76	1.12×10^{-4}	2.57	8.09×10^{-4}	2.74
1/64	1.69×10^{-5}	2.56	9.71×10^{-5}	2.81	1.83×10^{-5}	2.61	1.14×10^{-4}	2.83

Table 7
Estimated convergence rate for u and v at $t = 1$.

h	$\|u_{2h} - u_h\|_\infty$	r_u	$\|v_{2h} - v_h\|_\infty$	r_v
0.04	1.36×10^{-2}		1.87×10^{-2}	
0.02	3.30×10^{-3}	2.04	6.73×10^{-3}	1.47
0.01	8.11×10^{-4}	2.02	2.30×10^{-3}	1.55

$$r_q = \log_2 \frac{\|q_{4h} - q_{2h}\|_\infty}{\|q_{2h} - q_h\|_\infty}. \tag{47}$$

To test the convergence for the velocity components u and v, we use four grid lengths and run to time $t = 1$. The results are shown in Table 7. Typically the continuum surface force method leads to first-order convergence for the velocity, however, the results in here are better than that. Similar results were reported in [20].

Next we perform a numerical convergence study for our global numerical method by choosing the deformation factor $D(t)$ as the analyzing target. We take three grid lengths and run to time $t = 5$ for each case. Fig. 3 shows the curves of $D(t)$ and the estimated convergence rate. Numerical convergence for $D(t)$ is observed, and the estimated convergence rate $r(t)$ is higher than 1. The oscillation of $r(t)$ indicates that $r(t)$ may be time dependent.

4.3. Simulations in 2D

We present simulations on drop deformation (including a comparison with the small deformation theory), breakup and coalescence in 2D.

4.3.1. Drop deformation

For a moderate electric capillary number Ca_E, a drop can evolve into prolate or oblate shape in the steady state or remain spherical shape. For large Ca_E, the drop may break up into several small drops [49,32,22]. The 2D asymptotic analysis in [17] gives a small deformation expression to first-order as follows:

$$D \equiv \frac{L - B}{L + B} = \frac{f_d(\sigma, \epsilon)}{3(1 + \sigma)^2} Ca_E, \tag{48}$$

where L and B are the end-to-end lengths of the drop measured along the y-axis and the x-axis, respectively. $f_d(\sigma, \epsilon) = \sigma^2 + \sigma + 1 - 3\epsilon$ is a discriminating function. $f_d > 0, < 0$, or $= 0$ correspond to prolate, oblate, or circular shapes, respectively.

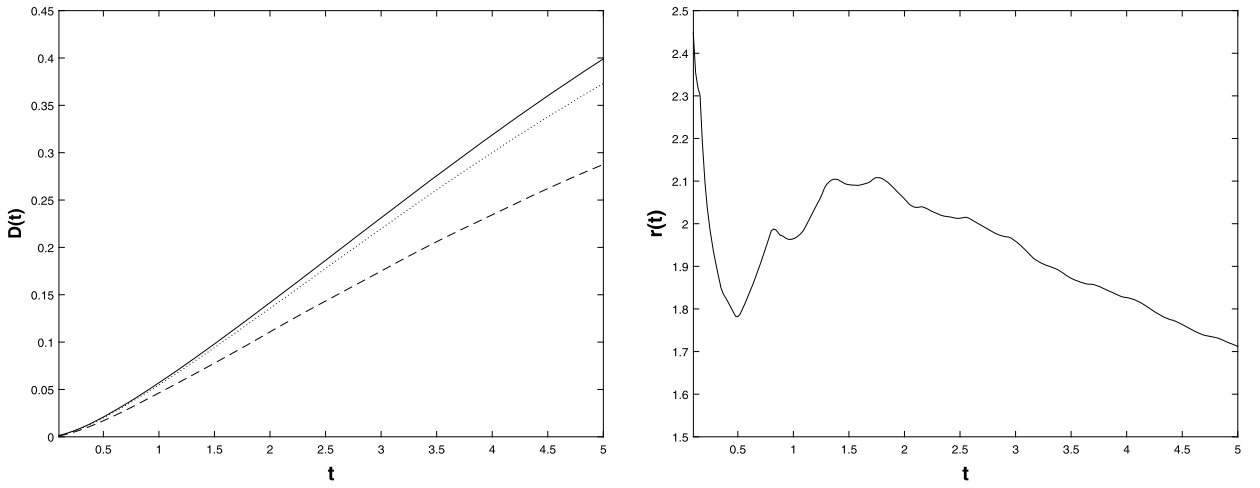

Fig. 3. Left: deformation factor as function of time for three grid lengths. $h = 0.02$ (solid line), 0.04 (dotted line) and 0.08 (dashed line); Right: the estimated convergence rate.

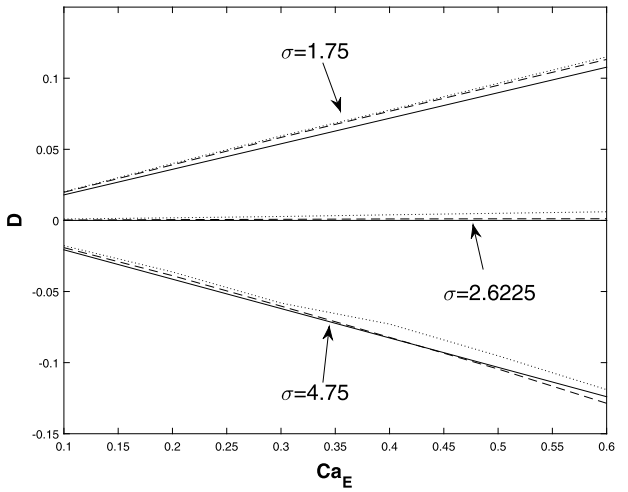

Fig. 4. Comparison between the small deformation theory and numerical simulations. Solid line: theoretical predication; dotted line: numerical prediction with mesh size 128×128; dashed line: numerical prediction with mesh size 256×256. In all cases $Oh = 1, \epsilon = 3.5$. $\Delta t = h/4$.

In simulations, the drop is a unit circle centered at the origin. $\Omega = [-4, 4]^2$. A comparison between the numerical calculation and the theoretical predication (48) is shown in Fig. 4. The numerical results agree well with the theoretical predications for small deformation, validating our numerical method in 2D. The discrepancy gets larger as Ca_E becomes larger because the theory is only valid for small deformation.

Under an electric field, a circulatory flow is generated to balance the electric stress in the steady state. For the oblate drop, the circulatory flow pattern inside the first quadrant is clockwise, while for the prolate one it can be either clockwise (if $\sigma < \epsilon$) or counterclockwise (if $\sigma > \epsilon$) (see, e.g., [20]). These flow patterns are observed in Fig. 5.

4.3.2. Drop breakup

Various drop breakup modes in EHD were studied in [22] under the assumptions of the axisymmetric geometry and Stokes creeping flow. Also assuming the axisymmetric geometry, the drop pinch-off mode was studied in [35], where the inertia effect was considered in [35]. Simulations in there were terminated right before the breakup.

We present an example of drop pinch-off in 2D. The parameter regime for the breakup can be different from that in [22,35] due to different spatial dimensions. The electric parameters are taken as $Oh = 1, Ca_E = 0.17, \sigma = 0.1, \epsilon = 2$. Initially the drop is a unit circle centered the origin. The simulation result is shown in Fig. 6. Under the electric field, the drop deforms into an oblate shape. Then the middle of the drop becomes thin, a neck region forms and the drop become a dumb bell. As the neck gets thinner and longer, the drop eventually breaks up into three daughter drops with the smallest in the middle.

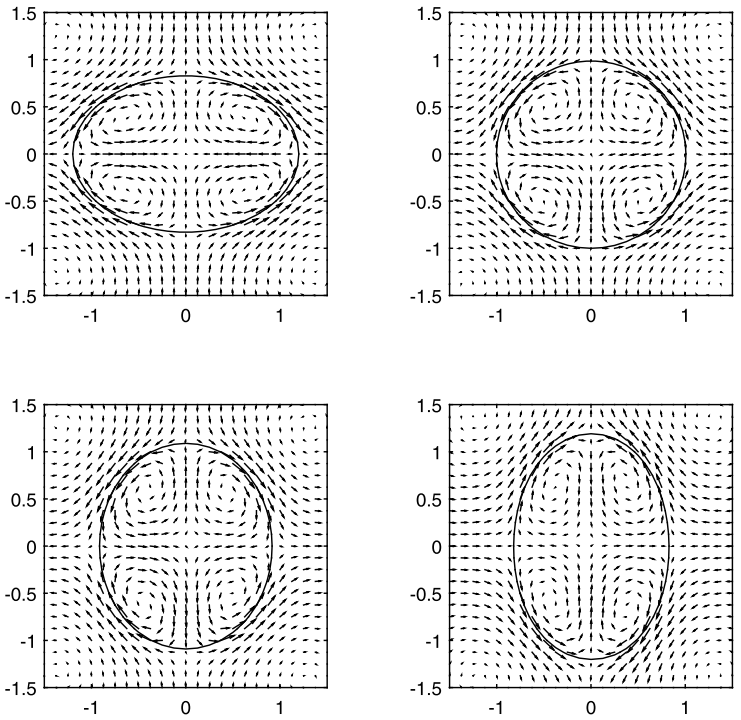

Fig. 5. Steady drop shape together with the velocity field at $t = 10$. Top left: oblate shape and clockwise flow (in the first quadrant, same in below) for $\sigma = 1.75$; Top right: circular shape and clockwise flow for $\sigma = 2.6225$; Bottom left: prolate shape and clockwise flow for $\sigma = 3.25$; Bottom right: prolate shape and counterclockwise flow for $\sigma = 4.75$. The other parameters: $\epsilon = 3.5$, $Oh = 1$, $Ca_E = 0.5$. Mesh size $= 128 \times 128$, $\Delta t = h/4$.

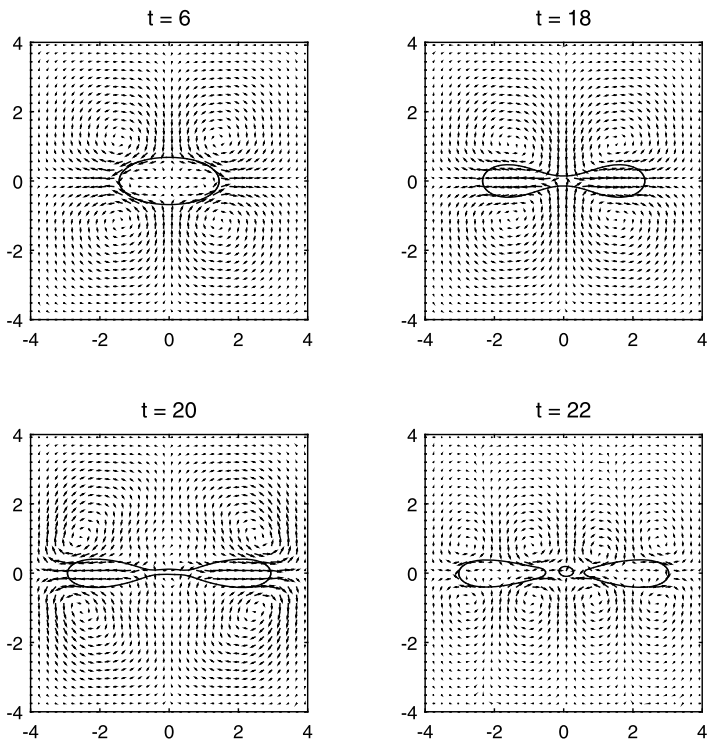

Fig. 6. Drop morphologies together with the velocity fields at different times. $h = 0.02$, $\Delta t = h/8$.

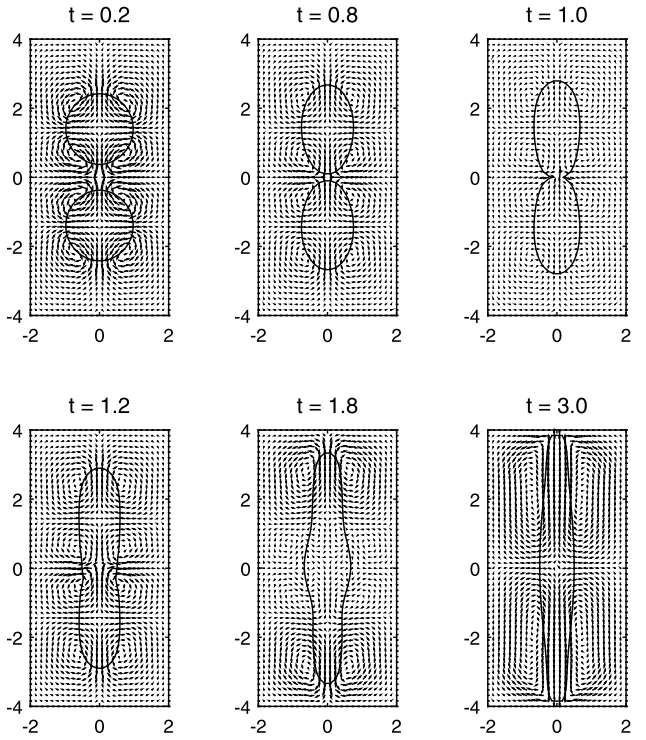

Fig. 7. Drop morphologies together with velocity fields at different times. $h = 0.02$, $\Delta t = h/4$.

4.3.3. Drop pair interaction

Drop pair interactions under electric fields were studied in [6] under the assumptions of Stokes creeping flow and axisymmetric geometry. In [6] the simulation was terminated just before the contact of two drops.

We consider that two drops of unit circle are aligned along y-axis and centered at $(0, \pm 1.4)$ respectively. The computational domain is $\Omega = (-2, 2) \times (-4, 4)$. The electric parameters are taken as $Ca_E = Oh = 1, \sigma = 4.75, \epsilon = 3.5$. Drop morphologies together with the velocity fields are shown in Fig. 7. In the process, two drops are deformed into prolate shape, approach to each other and merge into a large single drop. After the mergence, the kinked middle part of the drop swells until a lump forms. Then the drop is compressed in x-direction and stretches along y-direction, and drop shape becomes prolate.

This simulation together with the previous simulation of drop pinch-off demonstrates the capability of the level-set method in handling topological changes in 2D.

4.4. 3D simulations

In this section, we present fully 3D simulations on drop deformation, breakup and coalescence.

4.4.1. Comparison with small deformation theory

Asymptotic analysis in [49] gave the following first-order approximation to small drop deformation:

$$D = \frac{L - B}{L + B} = k_1 Ca_E, \tag{49}$$

where L and B are the major and minor axis from end-to-end of the deformed drop, respectively, with the major axis aligned with the applied electric field. And

$$k_1 = \frac{9}{16} \frac{\sigma^2}{(2+\sigma)^2} f_d,$$
$$f_d = \frac{\sigma^2 + \frac{3}{2}\sigma + 1 - \frac{7}{2}\epsilon}{\sigma^2}.$$

The above first-order approximation was extended to second-order in [2] as follows:

$$D = k_1 Ca_E + k_2 Ca_E^2, \tag{50}$$

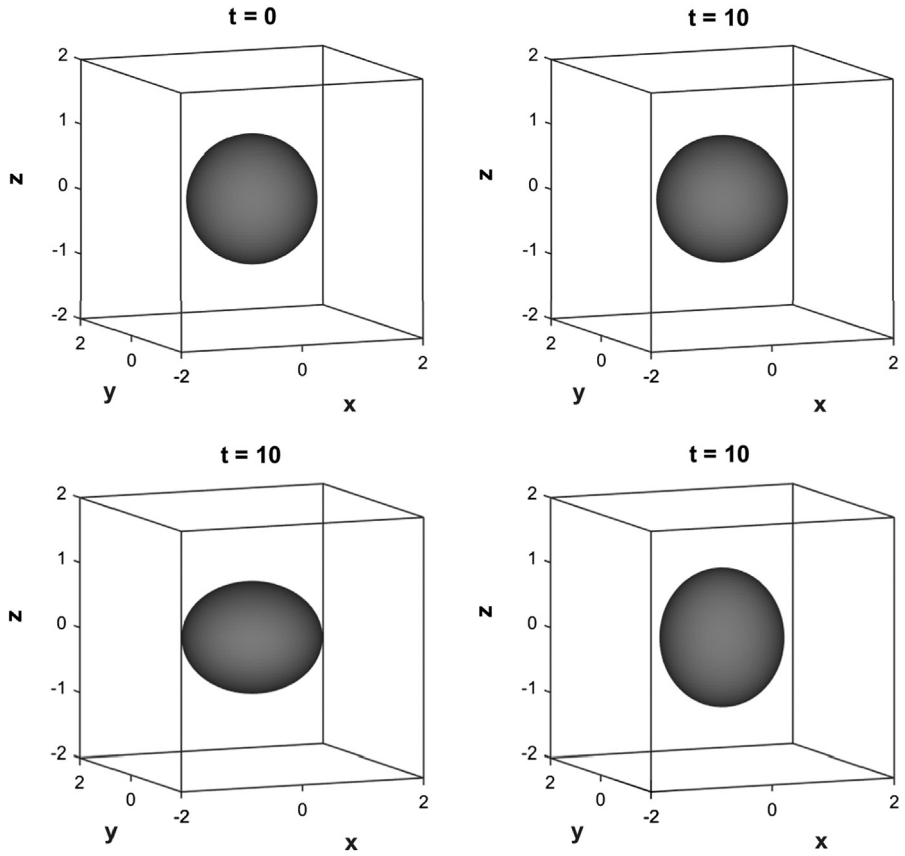

Fig. 8. Initial drop shape and the steady drop shapes for varied σ: $\sigma = 2.6869$ (top right), $\sigma = 1.5$ (bottom left), $\sigma = 4.5$ (bottom right). $Ca_E = 0.4$, $Oh = 1$, $\epsilon = 3.5$, $h = 1/16$, $\Delta t = h/4$.

where

$$k_2 = \frac{(139\sigma - 154)\sigma^2 f_d + 92(\sigma^2 + 2\sigma - (\sigma + 2)\epsilon)}{80(2+\sigma)^3} k_1.$$

Note that the viscosity ratio also plays a role in the deformation theory in [49,2]. In this work the viscosity ratio is assumed to be 1 for simplicity.

In simulations, the computational domain is $\Omega = (-4, 4)^3$. Initially the drop is a unit sphere centered at the origin. A drop can evolve into a steady oblate shape (if $f_d < 0$) or spherical shape (if $f_d = 0$) or prolate shape (if $f_d < 0$) as shown in Fig. 8.

A comparison with the above 3D small deformation theory for the oblate case is given in Fig. 9. It shows that the numerical predication agrees well with the theory.

4.4.2. Drop breakup

The computational domain is $\Omega = (-2, 2)^3$. Initially the drop is a unit sphere centered at the origin. The parameters are $Oh = 1, Ca_E = 0.3925, \sigma = 0.1, \epsilon = 2$. Similar to 2D simulations, the drop is compressed in z direction by the electric force, and consequently stretches in all horizontal directions. The middle of the drop keeps thinning until the drop pinches off. The snapshots of the droplet deformation are shown in Fig. 10. The results are similar to the axisymmetric simulations in [22,35].

In this simulation, we used a simple volume correction procedure to remedy the volume loss due to the numerical diffusion and/or the lack of resolution. The volume correction procedure was proposed in [28]. The idea is to expand slightly the zero level-set in its outward normal direction in each time step. Let V^0, V^n, L^n be the initial volume, the volume and the surface area t^n, respectively. Let ϕ^n be the level-set function obtained by solving the level-set equations, then we set

$$\phi^n := \phi^n - \epsilon_\phi, \quad \text{here} \quad \epsilon_\phi = \frac{V^0 - V^n}{L^n}. \tag{51}$$

The corrected level-set function ϕ^n is used in solving the N-S equations and the electric equations. The volume and the surface area are calculated by using the standard level-set techniques via the smoothed Heaviside function and the regularized

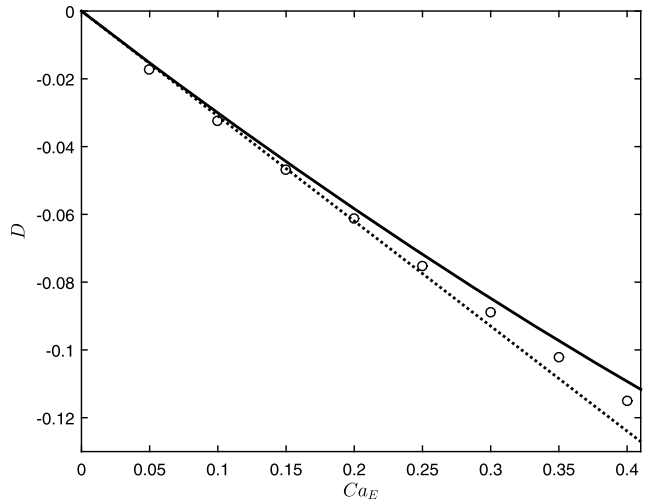

Fig. 9. A comparison with the small deformation theory. Solid line: second-order prediction; dotted-line: first-order prediction; circular points: numerical prediction. $\sigma = 1.5, \epsilon = 3.5, Oh = 1, h = 1/16, \Delta t = h/4$.

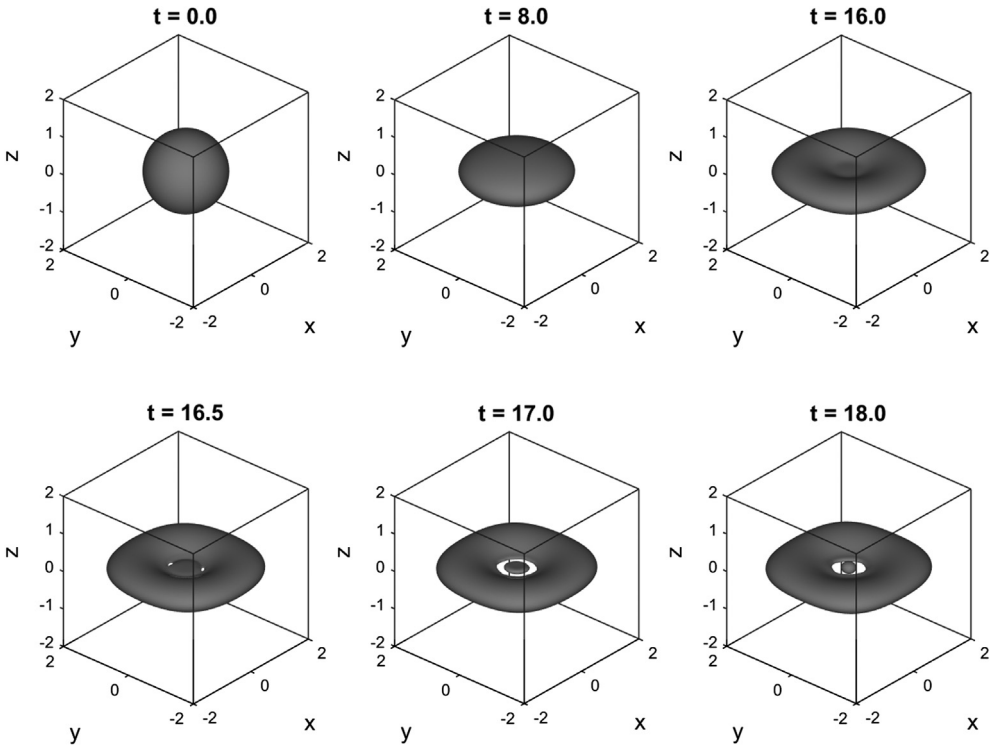

Fig. 10. Drop morphologies at different times. $h = 1/16, \Delta t = h/4$.

δ function, see, e.g., [53]. The correction parameter ϵ_ϕ is plotted as a function of time in Fig. 11. Its magnitude is less than 1.2×10^{-4} during the numerical evolution process.

4.4.3. Multiple drop interaction

Lastly we show a simulation on multiple drop interactions. The computational domain is $\Omega = (-2, 2) \times (-2, 2) \times (-6, 6)$. Initially three equally spaced unit spherical drops are aligned along z-axis and centered at $(0, 0, 0), (0, 0, \pm 3)$, respectively. The parameters are chosen as $\sigma = 4.75, \epsilon = 3.5, Ca_E = 2.0, Oh = 1$. The dynamic process of drop motion is shown in Fig. 12. Under the electric field, three drops are elongated in z-direction and become prolate. Drops approach and merge into a large drop. The merged drop keeps stretching. The calculation is terminated when the drop reaches the boundary.

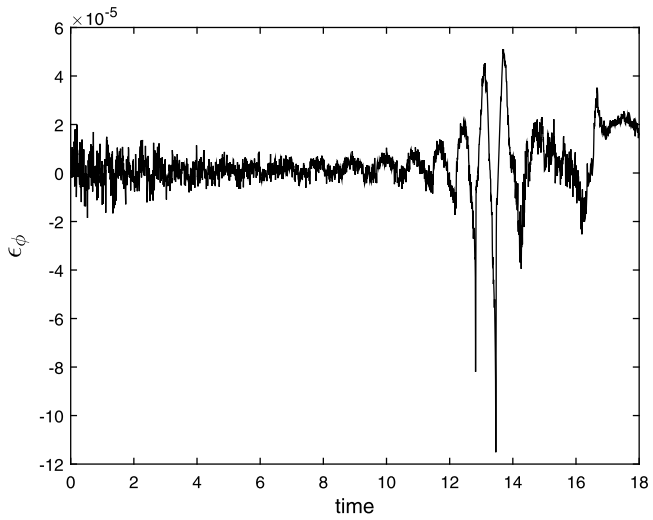

Fig. 11. The volume correction parameter as a function of time.

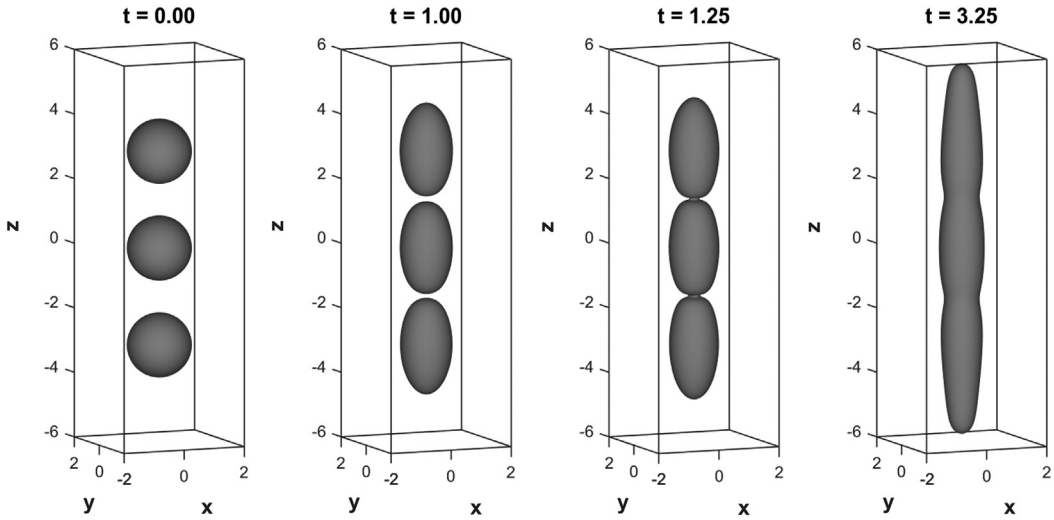

Fig. 12. Drop morphologies at different times. $h = 1/16$, $\Delta t = h/4$.

This example together the example of drop pinch-off show the capability of the level-set method in handling topological changes in 3D.

5. Conclusion

A level-set method has been presented for simulating the electrohydrodynamics using the leaky dielectric model. The electric potential Poisson equation is solved using a new version of the level-set based immersed interface method (IIM). The IIM avoids the local coordinate transform in literature and simplifies the algorithm significantly. Numerical examples indicate that the IIM achieves second-order accuracy in maximum norm for both the solution and its gradient for a wide range of diffusion coefficient ratios. The surface electric force is calculated using a level-set based extrapolation procedure, and the Navier-Stokes equations with singular surface forces is solved using the continuum surface force method. Numerical simulations on drop deformation, pinch-off and coalescence, are presented in both 2D and 3D. In particular, numerical simulations agree well with the small deformation theories. Simulations on the drop pinch-off and coalescence have demonstrated the capability of the level-set method in handling the interfacial topological changes.

In the future, we will extend the current method by including surfactant, and study the effect of surfactant on the electrohydrodynamics.

Declaration of competing interest

The authors declare that they have no known competing financial interests or personal relationships that could have appeared to influence the work reported in this paper.

Acknowledgement

We are grateful to the reviewer for the valuable comments.

References

[1] J. Adams, P. Swarztrauber, R. Sweet, Fishpack-a package of Fortran subprograms for the solution of separable elliptic partial differential equations, available at http://www.netlib.org/fishpack, 1980.
[2] O.O. Ajayi, A note on Taylor's electrohydrodynamic theory, Proc. R. Soc. Lond. A 364 (1978) 499–507.
[3] T.D. Aslam, A partial differential equation approach to multidimensional extrapolation, J. Comput. Phys. 193 (2003) 349–355.
[4] T.D. Aslam, S. Luo, H. Zhao, A static PDE approach for multidimensional extrapolation using fast sweeping methods, SIAM J. Sci. Comput. 36 (2014) A2907–A2928.
[5] O.A. Basaran, H. Gao, P.P. Bhat, Nonstandard inkjets, Annu. Rev. Fluid Mech. 45 (2013) 85–113.
[6] J.C. Baygents, N.J. Rivette, H.A. Stone, Electrohydrodynamic deformation and interaction of drop pairs, J. Fluid Mech. 368 (1998) 359–375.
[7] J.T. Beale, A.T. Layton, On the accuracy of finite difference methods for elliptic problems with interfaces, Commun. Appl. Math. Comput. Sci. 1 (2006) 91–119.
[8] T. Beale, A.T. Layton, A velocity decomposition approach for moving interfaces in viscous fluids, J. Comput. Phys. 228 (2009) 3358–3367.
[9] J.B. Bell, D.L. Marcus, A second-order projection method for variable-density flows, J. Comput. Phys. 101 (1992) 334–348.
[10] E. Bjorklund, The level-set method applied to droplet dynamics in the presence of an electric field, Comput. Fluids 38 (2009) 358–369.
[11] J.U. Brackbill, D.B. Kothe, C. Zemach, A continuum method for modeling surface tension, J. Comput. Phys. 100 (1992) 335–354.
[12] D.L. Brown, R. Cortez, M.L. Minion, Accurate projection methods for the incompressible Navier-Stokes equations, J. Comput. Phys. 168 (2001) 464–499.
[13] A. Castellanos, Electrohydrodynamics, Springer, 2014.
[14] D. Das, D. Saintillan, Electrohydrodynamics of viscous drops in strong electrical fields: numerical simulations, J. Fluid Mech. 829 (2017) 127–152.
[15] S. Deng, K. Ito, Z. Li, The three dimensional elliptic solvers for interface problems and applications, J. Comput. Phys. 184 (2003) 215–243.
[16] J.S. Eow, M. Ghadrir, Electrostatic enhancement of coalescence of water droplets in oil: a review of the technology, Chem. Eng. J. 85 (2002) 357–368.
[17] J.Q. Feng, A 2D electrohydrodynamic model for electrorotation of fluid drops, J. Colloid Interface Sci. 246 (2002) 112–121.
[18] A. Guittet, M. Lepilliez, S. Tanguy, F. Gibou, Solving elliptic problems with discontinuities on irregular domains – the Voronoi interface method, J. Comput. Phys. 298 (2015) 747–765.
[19] J-M. Hong, T. Shinar, M. Kang, R. Fedkiw, On boundary condition capturing for multiphase interfaces, J. Sci. Comput. 31 (2007) 99–125.
[20] W.-F. Hu, M.-C. Lai, Y.-N. Young, A hybrid immersed boundary and immersed interface method for electrohydrodynamics simulation, J. Comput. Phys. 282 (2015) 47–61.
[21] X. Huang, L. He, X. Luo, D. Yang, K. Shi, H. Yan, Breakup mode transformation of leaky dielectric droplet under direct current electric field, Int. J. Multiph. Flow 96 (2017) 123–133.
[22] E. Lac, G.M. Homsy, Axisymmetric deformation and stability of a viscous drop in a steady electric field, J. Fluid Mech. 590 (2007) 239–264.
[23] C.C. Langavant, A. Guittet, M. Theillard, F. Temprano-Coleto, F. Gibou, Level-set simulations of soluble surfactant driven flows, J. Comput. Phys. 348 (2017) 271–297.
[24] M.-C. Lai, A simple implementation of the immersed interface methods for Stokes flows with singular forces, Comput. Fluids 37 (2008) 99–106.
[25] A.T. Layton, A velocity decomposition approach for solving the immersed interface problem with Dirichlet boundary conditions, in: Natural Locomotion in Fluids and on Surfaces, 2012.
[26] R.J. LeVeque, Z. Li, The immersed interface method for elliptic equations with discontinuous coefficients and singular sources, SIAM J. Numer. Anal. 31 (1994) 1019–1044.
[27] Z. Li, A fast iterative algorithm for elliptic interface problems, SIAM J. Numer. Anal. 35 (1998) 230–254.
[28] Z. Li, S. Peng, Adaptive mesh refinement techniques for the immersed interface method applied to flow problems, Comput. Struct. 122 (2013) 249–258.
[29] Z. Li, M.-C. Lai, The immersed interface method for the Navier-Stokes equations with singular forces, J. Comput. Phys. 171 (2001) 822–842.
[30] Z. Li, K. Ito, The Immersed Interface Method: Numerical Solutions of PDEs Involving Interfaces and Irregular Domains, SIAM Front. Appl. Math., vol. 33, 2006.
[31] J. López-Herrera, S. Popinet, M.A. Herrada, A charge-conservative approach for simulating electrohydrodynamic two-phase flows using volume-of-fluid, J. Comput. Phys. 230 (2011) 1939–1955.
[32] J.R. Melcher, G.I. Taylor, Electrohydrodynamics: a review of the role of interfacial shear stress, Annu. Rev. Fluid Mech. 1 (1969) 111.
[33] C. Min, F. Gibou, A second-order accurate level set method on non-graded adaptive Cartesian grids, J. Comput. Phys. 225 (2007) 300–321.
[34] H. Minemawari, T. Yamada, H. Matsui, J. Tsutsumi, S. Haas, R. Chiba, R. Kumai, T. Hasegawa, Inkjet printing of single-crystal films, Nature 475 (2011) 364–367.
[35] H. Nganguia, Y.-N. Young, A.T. Layton, M.-C. Lai, W.-F. Hu, Electrohydrodynamics of a viscous drop with inertia, Phys. Rev. E 93 (2016) 053114.
[36] S. Osher, R. Fedkiw, Level Set Methods and Dynamic Implicit Surfaces, Applied Mathematical Sciences, vol. 153, Springer, 2003.
[37] S. Osher, J. Sethian, Fronts propagating with curvature-dependent speed: algorithms based on Hamilton-Jacobi formulations, J. Comput. Phys. 79 (1988) 12–49.
[38] D. Peng, B. Merriman, S. Osher, H.-K. Zhao, M. Kang, A PDE-based fast local level set method, J. Comput. Phys. 155 (1999) 410–438.
[39] C. Peskin, Numerical analysis of blood flow in the heart, J. Comput. Phys. 25 (1977) 220–252.
[40] C. Peskin, The immersed boundary methods, Acta Numer. 11 (2002) 479–517.
[41] Y. Saad, Iterative Methods for Sparse Linear Systems, PWS Publishing Company, 1996.
[42] D.A. Saville, Electrohydrodynamics: the Taylor-Melcher leaky dielectric model, Annu. Rev. Fluid Mech. 29 (1997) 27–64.
[43] W. Shi, J.-J. Xu, S. Shu, An adaptive semi-Langrangian level-set method for convection-diffusion equations on evolving interfaces, Adv. Appl. Math. Mech. 9 (2017) 1364–1382.
[44] C.-W. Shu, Essentially Non-Oscillatory and Weighted Essentially Non-Oscillatory Schemes for Hyperbolic Conservation Laws, Springer-Verlag, 1998.
[45] H.A. Stone, A.D. Stroock, A. Ajdari, Engineering flows in small devices: microfluidics toward lab-on-a-chip, Annu. Rev. Fluid Mech. 36 (2004) 381–411.
[46] J. Strain, Semi-Lagrangian methods for level set equations, J. Comput. Phys. 151 (1999) 498.
[47] M. Sussman, P. Smereka, S. Osher, A level-set approach for computing solutions of incompressible two-phase flow, J. Comput. Phys. 114 (1994) 146–159.

[48] Z. Tan, D. Le, Z. Li, K. Khoo, An immersed interface method for solving incompressible viscous flows with piecewise constant viscosity across a moving elastic membrane, J. Comput. Phys. 227 (2008) 9955–9983.
[49] G.I. Taylor, Studies in electrohydrodynamics I. The circulation produced in a drop by an electric field, Proc. R. Soc. Lond. A 291 (1966) 159.
[50] K.E. Teigen, S.T. Munkejord, Sharp-interface simulations of drop deformation in electric fields, IEEE Trans. Dielectr. Electr. Insul. 16 (2009) 475–482.
[51] K.E. Teigen, S.T. Munkejord, Influence of surfactant on drop deformation in an electric field, Phys. Fluids 22 (2010) 112110.
[52] G. Tomar, D. Gerlach, G. Biswas, N. Alleborn, A. Sharma, F. Durst, S.W.M. Welch, A. Delgado, Two-phase electrohydrodynamic simulations using a volume-of-fluid approach, J. Comput. Phys. 227 (2007) 1267–1285.
[53] J.-J. Xu, H. Zhao, An Eulerian formulation for solving partial differential equations along a moving interface, J. Sci. Comput. 19 (2003) 573–594.
[54] J. Xu, Z. Li, J. Lowengrub, H. Zhao, A level set method for interfacial flows with surfactant, J. Comput. Phys. 212 (2006) 590–616.
[55] J.-J. Xu, Y. Yang, J. Lowengrub, A level-set continuum method for two-phase flows with insoluble surfactant, J. Comput. Phys. 231 (2012) 5897–5909.
[56] J.-J. Xu, Y. Huang, M. Lai, Z. Li, A coupled immersed interface and the level-set method for 3D interfacial flows with insoluble surfactant, Commun. Comput. Phys. 15 (2014) 451–469.
[57] J.-J. Xu, W. Shi, M.-C. Lai, A level-set method for two-phase flows with soluble surfactant, J. Comput. Phys. 353 (2018) 336–355.
[58] S. Xu, An iterative two-fluid pressure solver based on the immersed interface method, Commun. Comput. Phys. 12 (2012) 528–543.
[59] J.-J. Xu, Level-Set Method for Two-Phase Flows with Surfactant, Scholars Press, 2018.